A Model for the FCC → HCP Transformation, Its Applications, and Experimental Evidence

S. MAHAJAN, M. L. GREEN, AND D. BRASEN

A model for the FCC → HCP transformation is proposed. It is envisaged that the dislocation reaction $a/2\ \langle 1\bar{1}0\rangle + a/2\ \langle 10\bar{1}\rangle \rightarrow 3 \times a/6\ \langle 2\bar{1}\bar{1}\rangle$ may govern the nucleation of six-layer HCP crystal. A macroscopic HCP region forms when these nuclei, located at different levels within a localized slipped region, grow into each other. The observed orientation dependence of the strain-induced martensite and the coexistence of HCP and twinned regions have been rationalized in terms of the proposed model. In addition, the supporting evidence has been developed by examining the crystallographic features of faulted regions in partially transformed Co-6.25 wt pct Fe alloy by transmission electron microscopy.

1. INTRODUCTION

THE FCC → HCP transformation is the simplest structural change, and can be accomplished by the passage of $1/6\ \langle 11\bar{2}\rangle$ Shockley partials on alternate $\{111\}$ planes as suggested by Christian.[1] The resulting $\{111\}$ interfaces between the transformed and untransformed regions are coherent in nature. It is a question of fundamental importance as to how the HCP crystals nucleate and grow in a well-annealed crystal. A consensus exists that lattice imperfections are involved in the transformation, but there is a considerable amount of disagreement regarding the mechanistic details. Following Fujita and Ueda,[2] different approaches can be broadly classified as follows: the mechanisms involving i) regular and ii) irregular overlapping of stacking faults. The models proposed by Basinski and Christian,[3] Bilby,[4] Seeger,[5,6] Bollman,[7] Hirth[8] and deLamotte and Altstetter[9] belong to the former category, whereas the suggestions of Fujita and Ueda[2] belong to the latter alternative.

The pole mechanism proposed by Basinski and Christian[3] has two limitations. Firstly, it requires the existence of HCP regions, and thus it cannot explain the early stages of the transformation as emphasized by the authors. Secondly, for a major dislocation, C[00.1], to act as a pole, it must extend from the existing HCP crystal into the adjoining FCC region. Since the dislocation is sessile, it is not clear how this is accomplished. Seeger's suggestions[5,6] do overcome the preceding difficulties, but the existence of the required dislocation configurations is extremely doubtful.

In order to rationalize the microstructural features observed in transformed Co, Bollman[7] has advanced a model based on intersecting faults. It is implicit in his suggestion that the total displacement associated with an HCP region $6n$ layers thick is essentially zero. However, deLamotte and Altstetter[9] and Kotval and Honeycombe[10] have shown experimentally that individual platelets in Co-30.5 wt pct Ni and Cu-12.5 wt pct Ge alloys are regions of high shear strains.

S. MAHAJAN and D. BRASEN are Member of Technical Staff and Associate Member of Technical Staff, respectively, Bell Laboratories, Murray Hill, NJ 07974. M. L. GREEN, formerly with Bell Laboratories, Murray Hill, NJ, is now with the Department of Materials Science and Engineering, Massachusetts Institute of Technology, Cambridge, MA 02139.

Manuscript submitted February 16, 1976.

Fujita and Ueda[2] visualize that stair-rod cross-slip plays an important role in the formation of HCP regions. Consider a situation where slip has occurred on the primary slip plane and glide dislocations are dissociated into Shockley partials. If stress on the intersecting glide plane is sufficiently high, the leading Shockley partial may dissociate into a stair-rod and a Shockley partial glissile on the intersecting plane. If this process is repeated on parallel planes separated by two layers, an HCP region could form.

The purpose of this paper is two-fold. Firstly, to propose an alternative mechanism for the nucleation and growth of thermally- and strain-induced HCP regions. Further, the observed coexistence of FCC twins and HCP regions[11-13] and the orientation dependence of strain-induced HCP martensite[14-16] have been rationalized in terms of the proposed model. Secondly, to present circumstantial evidence in support of the model obtained by correlating the crystallographic features of thermally-induced faults and slip structures in Co-6.25 wt pct Fe alloy by transmission electron microscopy.

2. A MODEL FOR TRANSFORMATION AND ITS APPLICATIONS

The formation of an HCP region can be envisaged to occur in two stages: i) nucleation of an embryo; and ii) its subsequent growth into a macroscopically observable size. It is proposed that two $a/2\ \langle 110\rangle$ dislocations of different, but coplanar, Burgers vectors can interact according to the following reaction to form a six-layer HCP region:

$$\frac{a}{2}\langle 1\bar{1}0\rangle_{\{111\}} + \frac{a}{2}\langle 10\bar{1}\rangle_{\{111\}} \rightarrow 3 \times \frac{a}{6}\langle 2\bar{1}\bar{1}\rangle_{111}.$$

An identical dislocation reaction has been shown likely to be responsible for the nucleation of three-layer twins in FCC crystals.[17]

For instance, consider the situation when an $a/2\ [10\bar{1}]$ dislocation approaches an $a/2\ [1\bar{1}0]$ dislocation from the left as shown in Fig. 1(a); both the dislocations are dissociated into the respective Shockley partials and are gliding on the (111) plane. The interaction between the two dislocations is repulsive in nature, but it could be changed locally into an attractive one by swapping the positions of P_3 and P_4. This swap-over could occur either at an existing constriction or at a constriction formed during the interaction.[18] In order to avoid anomalous faulting, P_3 and P_4 must in turn dissociate as follows:

$$P_3 \equiv \frac{\mathbf{a}}{6}[2\bar{1}\bar{1}] \rightarrow \frac{\mathbf{a}}{6}[1\bar{2}1] + \frac{\mathbf{a}}{6}[11\bar{2}]$$

$$P_4 \equiv \frac{\mathbf{a}}{6}[11\bar{2}] \rightarrow \frac{\mathbf{a}}{6}[\bar{1}2\bar{1}] + \frac{\mathbf{a}}{6}[2\bar{1}\bar{1}].$$

It is envisaged that if the material is undergoing deformation below its M_d temperature, the faults may rearrange themselves into a four-layer HCP crystal as illustrated in Fig. 1(*b*). It is emphasized that the transformation of the situation shown in Fig. 1(*a*) into the one depicted in Fig. 1(*b*) involves the rearrangement of atoms within the cores of the Shockley partials. This is likely to be facilitated by the higher thermodynamic stability of the HCP phase. Finally, the four-layer HCP region shown in Fig. 1(*b*) could transform into a six-layer thick HCP crystal, Fig. 1(*c*), during the interaction of the former with another four-layer or six-layer nucleus. The analogous situation has previously been discussed in the context of FCC twinning.[17] Furthermore, it is recognized that the fault arrangement shown in Fig. 1(*c*) would likewise arise if the $\mathbf{a}/2\ [10\bar{1}]$ and $\mathbf{a}/2\ [1\bar{1}0]$ dislocations were gliding on adjacent planes instead of being coplanar. Alternatively, the arrangement shown in Fig. 1(*c*) could arise via a scheme involving the cross glide of $\mathbf{a}/2\ [10\bar{1}]$ dislocation and the nucleation of $\mathbf{a}/6\ [\bar{1}2\bar{1}]$ and $\mathbf{a}/6\ [2\bar{1}\bar{1}]$ Shockley partial loops on the appropriate planes.

A macroscopically observable HCP region could form when six-layer nuclei located at different levels within a deformed region grow into each other. Nourtier and Saada[19] have shown that the presence of stacking faults may produce long range electronic perturbations in the lattice. It is reckoned that, due to these electronic interactions, the distribution of stacking faults and six-layer nuclei within the slip band is localized and thus the probability of a particular slipped region to evolve into a macroscopic HCP crystal is enhanced. Furthermore, as a result of the cross slip, two dislocations should be capable of forming HCP nuclei at different levels within the slip band. Consequently, the number of dislocations required to form a macroscopic HCP crystal may be substantially reduced. In addition, it is very likely that the two dislocations are not always associated with each other, but they are dissociated into the respective Shockley partials. Under those circumstances their absorption into the HCP crystal may lead to a faulted structure. The randomly distributed faults observed in HCP Co by Edwards and Lipson[20] and Wilson[21] could be a consequence of this effect.

Let us now visualize some of the *simple* situations which could develop during the coalescence process. In Fig. 2(*a*), the two nuclei are at the same level within the slip band. It is apparent that, when they coalesce, the thickness of the HCP crystal remains the same. The only perceptible change entails the formation of the $\mathbf{a}/2\ [1\bar{1}0]$ and $\mathbf{a}/2\ [10\bar{1}]$ dislocations within the HCP crystal. If, on the other hand, the two nuclei are displaced with respect to each other by one layer, their intergrowth leads to a six-layer twin as shown in Fig. 2(*b*). It is envisaged that FCC twins occurring concomitantly with the HCP regions[11-13] may be rationalized in terms of the preceding situation. It is emphasized that the formation of FCC twins is very difficult to comprehend via the pole models for the transformation,[3-6] whereas it evolves

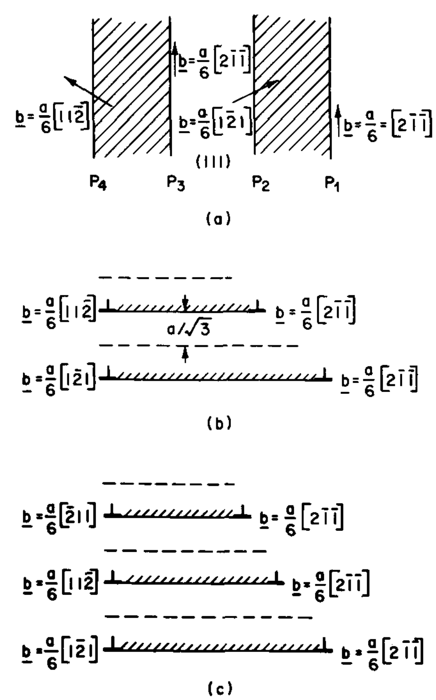

Fig. 1—(*a*) A planar view of a situation which could result from the dissociation of $\mathbf{a}/2[1\bar{1}0]$ and $\mathbf{a}/2[10\bar{1}]$ dislocations into Shockley partials on the (111) plane. (*b*) and (*c*) Schematics of the four- and six-layer HCP crystals which may evolve from the situation shown in (*a*).

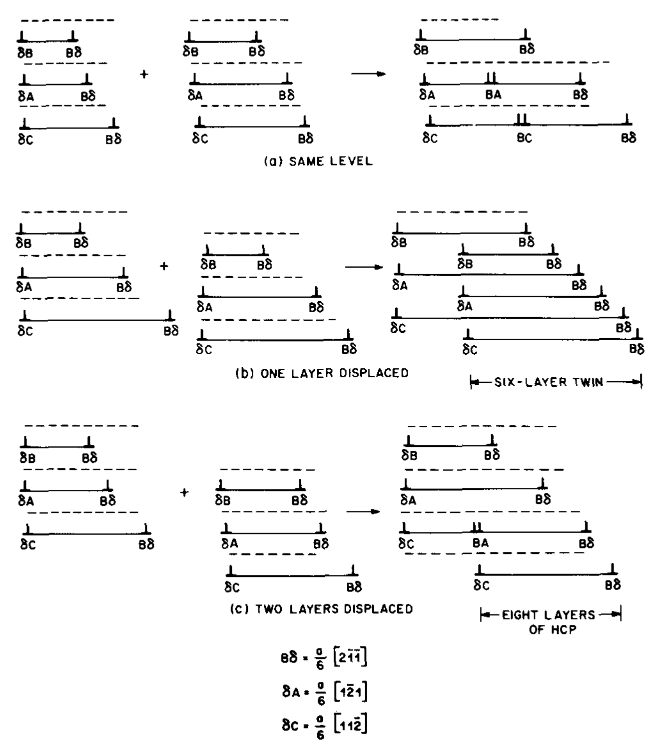

Fig. 2—Possible configurations resulting from the coalescence of six-layer HCP nuclei: (*a*) nuclei on the same level, (*b*) one layer apart and (*c*) two layers apart.

as a natural consequence in the present situation. Furthermore, twins cannot be regarded as the accommodation substructure because both the twinned and transformed regions have identical shear vectors. Let us now consider the case when the two nuclei are displaced with respect to each other by two layers. Their agglomeration results in an eight-layer thick HCP crystal, Fig. 2(*c*). It is relatively easy to visualize that depending upon the relative displacement between the two nuclei, HCP regions and twins of different thicknesses can form.

An interesting question concerning the formation of twins may arise. Since the agglomeration of the nuclei in Fig. 2(*b*) results in a phase of the lower thermodynamic stability, then what factor is responsible for the intergrowth. The answer to this question is not clear. A possible explanation could be that the force experienced by the partials due to the applied stress may overcome the resistive force due to the free energy difference between the FCC and HCP phases.

Stone and Thomas[16] have investigated in detail the orientation dependence of deformation-induced HCP martensite in Fe-15 wt pct Ni-15 wt pct Cr alloy single crystals. One of their observations is at variance with that of Lagneborg[14] and Goodchild *et al.*[15] Stone and Thomas observe that when the tensile axis is parallel to [100], the HCP martensite forms on two variants, whereas the latter investigators notice the absence of the martensite in grains oriented along their [100] direction. No satisfactory explanation can be given for this discrepancy. In addition, it is observed that when the axis is parallel to $[\bar{1}\bar{1}2]$, the martensite forms on the $(1\bar{1}1)$ and $(\bar{1}11)$ planes, while for the $[\bar{2}\bar{1}3]$ orientation the habit plane is $(\bar{1}11)$. This can be rationalized as follows. When the axis is parallel to $[\bar{1}\bar{1}2]$, $\pm\mathbf{a}/2\ [\bar{1}01](1\bar{1}1)$ and $\pm\mathbf{a}/2\ [0\bar{1}1](\bar{1}11)$ slip systems will be activated. Based on the observations of Pande and Hazzledine,[22] the secondary slip vector on both planes is likely to be $\pm\mathbf{a}/2\ [\bar{1}\bar{1}0]$. The $\pm\mathbf{a}/2\ [\bar{1}\bar{1}0]$ dislocations could react with the primary slip vectors, according to the proposed model, to form HCP regions on the $(1\bar{1}1)$ and $(\bar{1}11)$ planes. For the $[\bar{2}\bar{1}3]$ orientation, the primary and secondary slip systems to be activated are $\pm\mathbf{a}/2\ [0\bar{1}1](\bar{1}11)$ and $\pm\mathbf{a}/2\ [\bar{1}\bar{1}0](\bar{1}11)$. Again, the two slip vectors could interact to form martensite on the $(\bar{1}11)$ plane.

In the foregoing, no clear-cut distinction has been made between the deformation- and thermally-induced HCP martensites. Crystallographically and structurally they are likely to be identical as deduced by Kotval and Honeycombe,[10] but an obvious question concerns the source of stress in the case of thermal transformation. Following Friedel,[23] the free energy difference between the FCC and HCP phases can be likened to an imposed stress. This stress can, however, only be realized after the formation of the first nucleus. At this juncture it is not clear as to how the initial transformation is triggered. It could be that in the vicinity of the existing imperfections the FCC lattice may become unstable and transform over to the stable HCP phase.

The assignment of Burgers vectors to the partials constituting the noncoherent interface of the six-layer nucleus is shown in Fig. 1(*c*). These dislocations are a geometrical necessity because the faulted regions terminating inside the crystal must be bounded by partials. Since the sum of the Burgers vectors of the partials forming the left, noncoherent interface is zero, these partials will not experience any force due to an applied stress. Consequently, the three partials on the left-hand side will not glide under the influence of the applied stress, whereas Shockley partials on the right could glide away from the reaction junction and thus expand the HCP region.

3. EXPERIMENTAL DETAILS

Since Co transforms extensively on cooling to room temperature and the Fe additions tend to stabilize the FCC phase, it was decided to use a Co-Fe alloy for investigating the structural characteristics of the thermally-induced transformation. A preliminary study involving optical metallography established that Co-6.25 wt pct Fe alloy would be a suitable composition. The alloy was prepared by induction melting and cast into an ingot. The ingot was swaged into a 1/4 in. diam rod which was subsequently rolled into 0.010 in. thick strip. The strip samples were annealed for an extended period at 1100°C and then air cooled. To prepare thin foils suitable for microscopy, the strips were thinned to 0.004 in. in a solution consisting of equal volumes of H_3PO_4 and H_2O_2. Chemically polished samples were subsequently electropolished, using the window technique, in an 80 pct CH_3OH-$HClO_4$ solution maintained at −30°C. Suitable sections were cut from the thinned samples and examined in a JEM 200 microscope operating at 200 kv. Since the alloy is ferromagnetic and distorts the electron beam, very small sections were examined. In all cases the upward normal of the region being examined was indexed in a self-consistent manner during examination from the Kikuchi line pattern superimposed on the spot pattern.

4. RESULTS AND ANALYSIS

4.1. Characterization of Some Fault Configurations

4.1.1. Case I. Fig. 3 shows isolated faults F_1 and F_2 and some fault-clusters, F_3, F_4 and F_5, which have not yet evolved into a macroscopic HCP region. It appears that F_1 grows from a defective area in the boundary between Grains *A* and *B*. F_2 also appears to extend from the same area into the adjoining Grain *B*. Since the boundary is invisible for $\mathbf{g} = \bar{1}1\bar{1}$, its residual trace appears edge-on in Fig. 3(*b*) and the $[\bar{1}1\bar{1}]$ vector is normal to its residual trace, the interface between Grains *A* and *B* could be a coherent twin boundary (CTB) lying on the $(\bar{1}1\bar{1})$ plane.

F_1 exhibits fault contrast for $\mathbf{g} = 200$, $\bar{1}1\bar{1}$ and $\bar{2}20$ and invisible for $\mathbf{g} = 02\bar{2}$, while F_3, F_4 and F_5 are visible for $\mathbf{g} = 200$ and $\bar{1}1\bar{1}$ and invisible for $\mathbf{g} = \bar{2}20$ and $02\bar{2}$. Based on these observations, $(\bar{1}11)$ and (111) habits can be assigned to F_1 and F_3, F_4 and F_5, respectively.

F_1 appears to terminate on another fault which lies on the $(\bar{1}\bar{1}1)$ plane; the latter is normal to the plane of the micrograph in Fig. 3(*b*). The preceding assessment is borne out by the experimental observations. Since the habit plane of F_1 and the $(\bar{1}\bar{1}1)$ plane inter-

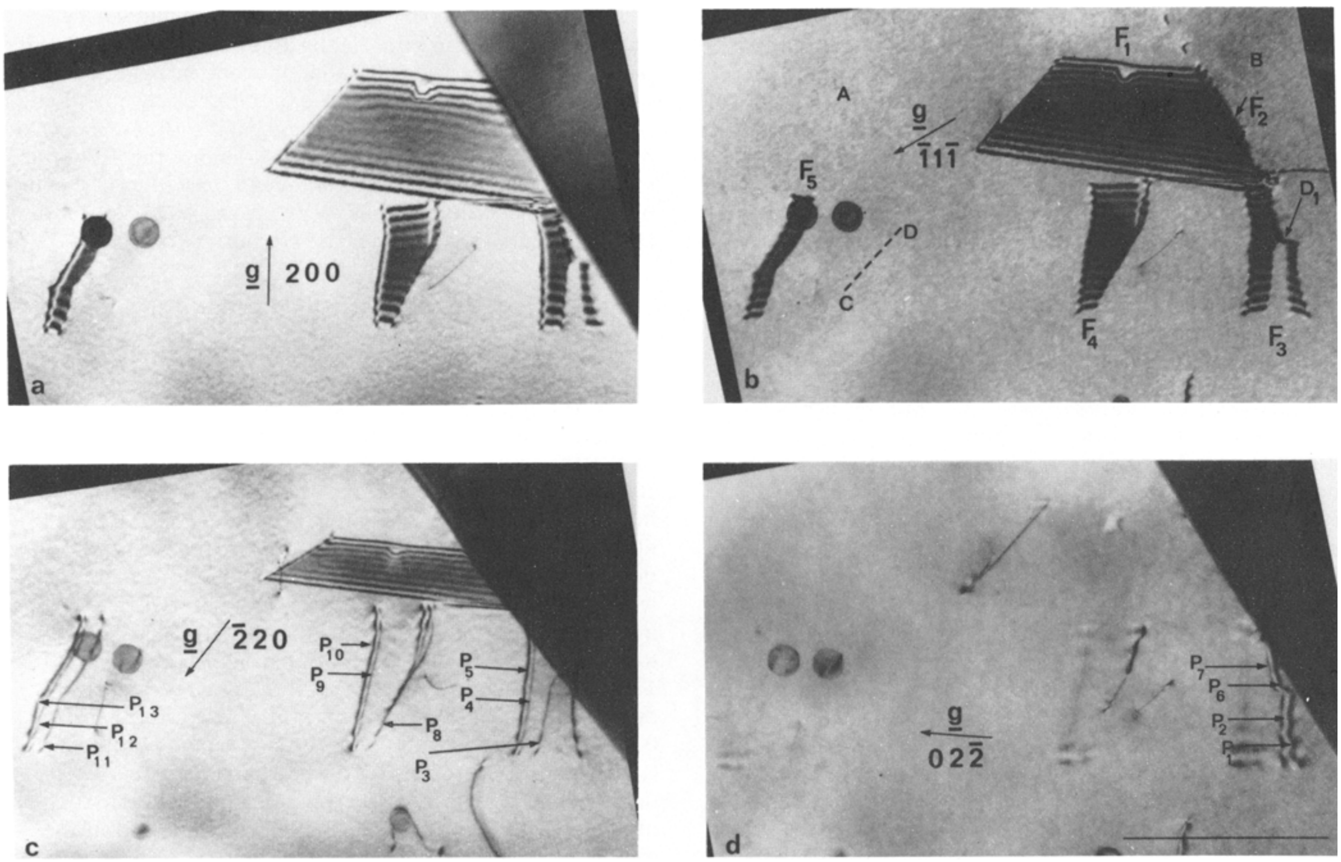

Fig. 3—Micrographs illustrating the contrast behavior of various structural features comprising Case I. The planes of the micrographs (*a*), (*b*), (*c*) and (*d*) are ~(011), ~(011), ~(111) and ~(011), respectively. *CD* refers to the projection of the line of intersection of the $(\bar{1}11)$ and $(\bar{1}\bar{1}1)$ planes onto the (011) plane. The marker represents 1 μ.

sect along [101], its projection onto the (011) plane should lie along the $[2\bar{1}1]$ direction. The observed projection, *CD*, indeed coincides with that.

The Burgers vectors of partials bounding F_3, F_4 and F_5 can be ascertained from Fig. 3. Partials P_3, P_4, P_5, P_8, P_9, P_{10}, P_{11}, P_{12} and P_{13} are in contrast for $\mathbf{g} = \bar{2}20$ and invisible for $\mathbf{g} = 02\bar{2}$. On the other hand, P_2, P_6 and P_7 are in contrast for $\mathbf{g} = 02\bar{2}$ and invisible for $\mathbf{g} = \bar{2}20$, while P_1 is visible for $\mathbf{g} = \bar{2}20$ and $02\bar{2}$. Since F_3, F_4 and F_5 lie in the (111) plane, $\pm\mathbf{a}/6\ [\bar{2}11]$, $\pm\mathbf{a}/6\ [11\bar{2}]$ and $\pm\mathbf{a}/6\ [1\bar{2}1]$ Burgers vectors can be assigned to P_3, P_4, P_5, P_8, P_9, P_{10}, P_{11}, P_{12} and P_{13}, P_2, P_6 and P_7 and P_1, respectively. Bearing in mind the modifications which occur in the contrast behavior of the partials bounding multilayer faults for $|\mathbf{g}\cdot\mathbf{b}_p| = 2/3$ and $1/3$,[24-27] where $\mathbf{b}_p$ is the Burgers vector of the partial, the observed contrast for $\mathbf{g} = \bar{1}1\bar{1}$ and 200 is consistent with the preceding Burgers vector assignation. Also, it is apparent from Fig. 3 that the Burgers vector of dislocation D_1 is $\pm\mathbf{a}/2\ [0\bar{1}1]$.

The character of different faults has been ascertained by following the procedure developed by Hashimoto, Howie and Whelan.[28] It is inferred that the faults defined by P_1 and P_2, P_3 and P_4, P_8 and P_9 and P_{11} and P_{12} are intrinsic in nature, while those defined by P_4 and P_5, P_6 and P_7, P_9 and P_{10} and P_{12} and P_{13} are extrinsic in character. However, it cannot be established by the present experiments whether or not the two intrinsic faults constituting the extrinsic faults are contiguous to each other or have a layer of unfaulted crystal between (see Fig. 1(*b*)). Thermodynamically, the latter configuration is more likely because it produces the more stable HCP phase. Consequently, it will be assumed in the present work that the fault configurations, such as the left-hand portion of F_3, F_4 and F_5, are identical to the one shown in Fig. 1(*b*) and we will designate these as "pseudo" fault-pairs.

4.1.2. Case II. Fig. 4 illustrates how dislocations D_2 and D_3 can interact with D_4, which is out of contrast, to form pseudo fault-pairs F_6 and F_7. The evolution of F_6 involves the intersection between D_2 and D_4, while to form F_7, D_3 and D_4 align themselves into a nearly parallel arrangement. These situations have recently been evaluated with regard to the development of fault-pairs.[18] Furthermore, the fault configurations F_8, F_9 and F_{10} are identical to F_6 and F_7 except that they have propagated more extensively. F_{10} also appears to terminate on a well-developed, faulted region lying on the $(\bar{1}1\bar{1})$ plane. Since the preceding features were observed in a relatively thicker part of the crystal, it proved almost impossible to carry out detailed contrast experiments.

4.1.3. Case III. Fig. 5 shows the development of a localized slipped region containing numerous faults bounded by partials P_{14}, P_{15}. . . P_{37}. The extent of the slipped area is defined by the boundary between Grains *E* and *F* and a transformed region *G*, see Fig. 5(*c*). On the basis of the trace analysis and the contrast behavior shown in Fig. 5, it is inferred that

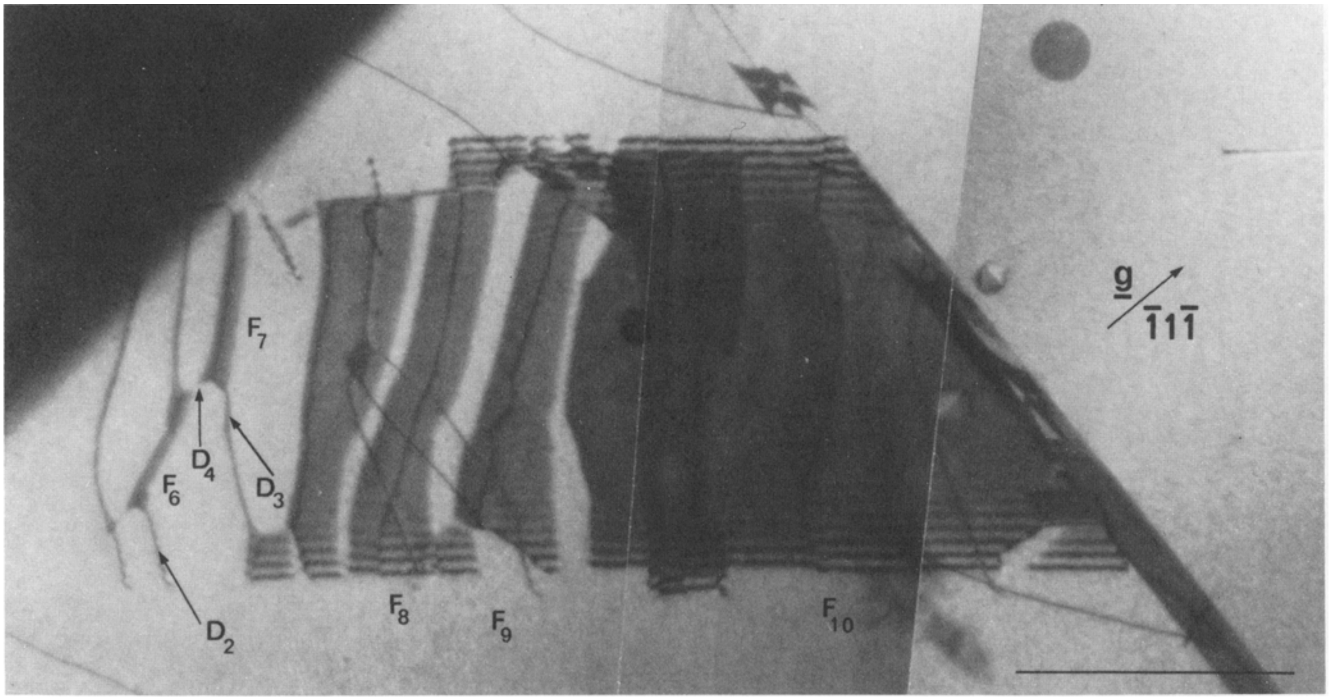

Fig. 4—Micrograph illustrating the formation of faulted structures *via* the dislocation-dislocation interaction envisaged in the model (Case II). The plane of micrograph is ~(011). The marker represents 1 μ.

the interface between Grains E and F is a ($\bar{1}1\bar{1}$) CTB. Similarly, the habit plane of G is identified to be ($11\bar{1}$).

The fault contrast is observed for $\mathbf{g} = 11\bar{1}$ and $\bar{2}00$, but is invisible for $\mathbf{g} = 0\bar{2}2$ and $\bar{2}02$. These observations are consistent with the assignation of the (111) habit to these structural features. This is indeed borne out by the trace analysis.

An interesting observation concerns the presence of light fringes between P_{24} and P_{25}, P_{26} and P_{27}, P_{28} and P_{33} and P_{34} and P_{35}, see Fig. 5(a). Similar fringes appear to be present between the boundary between Grains E and F and P_{15} and P_{17} and P_{18}, but they are not readily discernible. These light fringes have previously been reported in deformed Cu-8 at. pct Si (Ref. 29) and Mo-35 at. pct Re alloys,[30,31] and have been attributed to the presence of twins $3n$ layers thick, where n is an integer. We believe that an identical explanation holds in the present situation, except now the $3n$ faults are appropriately separated from each other so as to form a $6n$-layer thick HCP region.

Partials P_{14}, P_{31} and P_{34} (Group I) are in contrast for $\mathbf{g} = 0\bar{2}2$ and $\bar{2}02$; P_{15}, P_{16}, P_{17}, P_{18}, P_{19}, P_{21}, P_{23}, P_{26}, P_{28}, P_{30}, P_{32}, P_{33} and P_{35} (Group II) are in contrast for $\mathbf{g} = \bar{2}02$, but are invisible for $\mathbf{g} = 0\bar{2}2$; P_{20}, P_{22}, P_{25}, P_{27} and P_{29} are in contrast for $\mathbf{g} = 0\bar{2}2$ and are invisible for $\mathbf{g} = \bar{2}02$. It has been confirmed from ancillary observations not shown in Fig. 5 that P_{36} and P_{37} also belong to Group II. Since the faults lie on the (111) plane, these results are compatible with the assignation of $\pm\mathbf{a}/6\ [11\bar{2}]$, $\pm\mathbf{a}/6\ [\bar{2}11]$ and $\pm\mathbf{a}/6\ [1\bar{2}1]$ Burgers vectors to Group I, II and III partials, respectively. Also, based on the results shown in Fig. 5, the following characters can be assigned to different faults: the faults defined by P_{14}, P_{15} and P_{16}, P_{18} and P_{19}, P_{20} and P_{21}, P_{22} and P_{23}, P_{33} and P_{34}, and P_{35} and P_{36} are intrinsic in nature, while those defined by P_{16} and P_{17}, P_{19} and P_{20}, P_{21} and P_{22}, P_{23} and P_{24}, P_{25} and P_{26}, P_{27} and P_{28}, P_{29} and P_{30}, P_{31} and P_{32} and P_{36} and P_{37} are extrinsic in character. Furthermore, comparing Fig. 5(a) and (c) it is evident that during the examination, certain configurational changes occur in the faults bounded by P_{31} and P_{32} and P_{33} and P_{34}. A constriction which is observed in Fig. 5(a) is no longer visible in Fig. 5(c), and the character of the lower portion of the fault changes from intrinsic to extrinsic. This is consistent with the mechanism recently proposed for the transformation of an intrinsic fault into an extrinsic fault.[18]

Dislocation or ledge HI is visible in Fig. 5(d). Its projection onto the (111) plane lies along $[\bar{1}01]$, which in turn is the projection of the line of intersection of the ($1\bar{1}1$) and (111) planes. It is therefore envisaged that the closely spaced $\pm\mathbf{a}/6\ [\bar{2}11]$ partials constitute HI. These partials could have comprised the interface of the $6n$-layer thick HCP region and may have been pushed against the ($\bar{1}1\bar{1}$) CTB during its growth.

For the sake of clarity, the preceding results have been summarized in Fig. 6. It is again emphasized that the assumed "pseudo" extrinsic character for various faults cannot be differentiated from a situation where two intrinsic faults are next to each other.

4.1.4. Case IV. Fig. 7 shows another localized slipped region containing a few faults which are delineated by partials $P_{38} \ldots P_{43}$. The fault contrast is observed for $\mathbf{g} = \bar{1}1\bar{1}$, $11\bar{1}$, 200 and $\bar{2}20$ and is invisible for $\mathbf{g} = 02\bar{2}$. Assuming that the transformation occurs via the $\pm 1/6\langle 11\bar{2}\rangle\{111\}$ shear, these observations are consistent with the ($\bar{1}11$) habit for these faults. Also, the following characters can be assigned to different faults: the faults defined by P_{38} and P_{39}, P_{40} and P_{41} and P_{42} and P_{43} are intrinsic in nature, whereas that defined by P_{39} and P_{40} is extrinsic in character. Furthermore, P_{41} and P_{42} define a region which exhibits light fringes. This may imply that the area is a $6n$-layer thick HCP region. Based on the diffraction contrast behavior of the partials, $\pm a/6\ [\bar{1}1\bar{2}]$, $\pm a/6\ [211]$ and $\pm a/6\ [\bar{1}\bar{2}1]$ Burgers vectors can be assigned to P_{38} and P_{39}, P_{40} and P_{41} and P_{42} and P_{43}, respectively. A possible configurational arrangement for different partials, consistent with the preceding results, is shown in Fig. 8. There are other microstructural features on the micrograph, see Fig. 7(d). They appear to be a result of the slip activity on the $(11\bar{1})$ planes.

4.2. Role of Grain Boundaries

In the present experiments, the role of grain boundaries in the transformation could not be evaluated unequivocally. However, there are some observations which indicate that faults could nucleate from imperfections present in the boundaries. Fig. 9(a) shows one such example. Faults F_{11} and F_{12} appear to form from the boundary substructure. It is, however, not clear whether or not F_{13} nucleated from the boundary or terminated on it. Fig. 9(b) shows another situation where a transformed region F_{14}, lying on the $(1\bar{1}1)$ planes, appears to grow from a non-

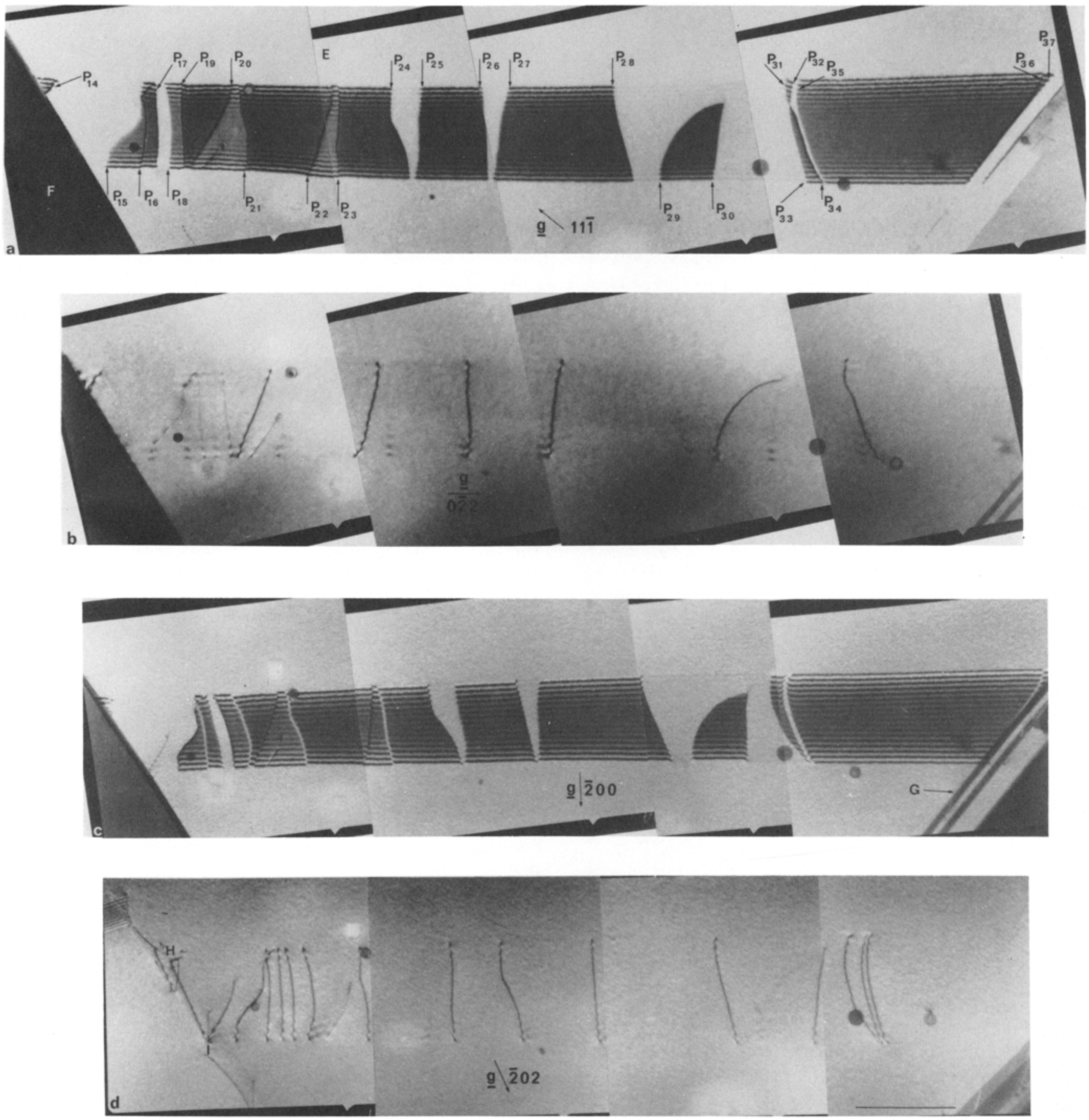

Fig. 5—Micrographs illustrating the contrast behavior of various structural features comprising Case III. The planes of the micrographs (a), (b), (c) and (d) are ~(011), ~(011), ~(011) and ~(111), respectively. Dislocation HI lies along the line of intersection of the $(1\bar{1}1)$ and (111) planes. The marker represents 1 μ.

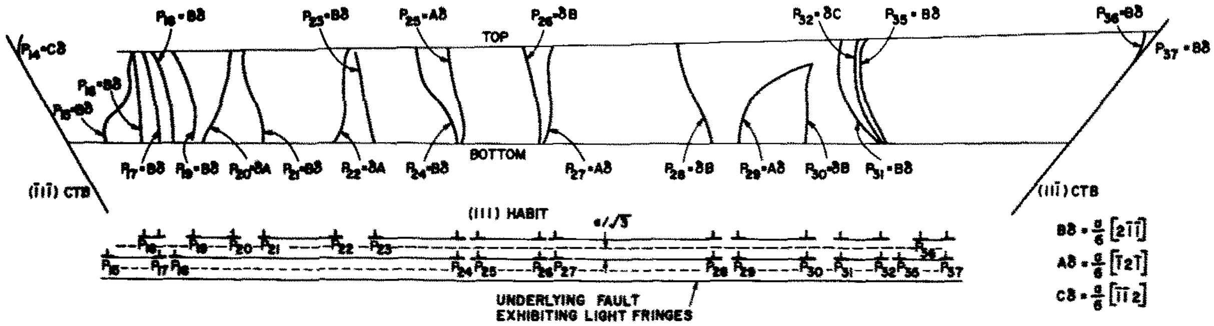

Fig. 6—A possible configurational arrangement of the structural features shown in Fig. 5.

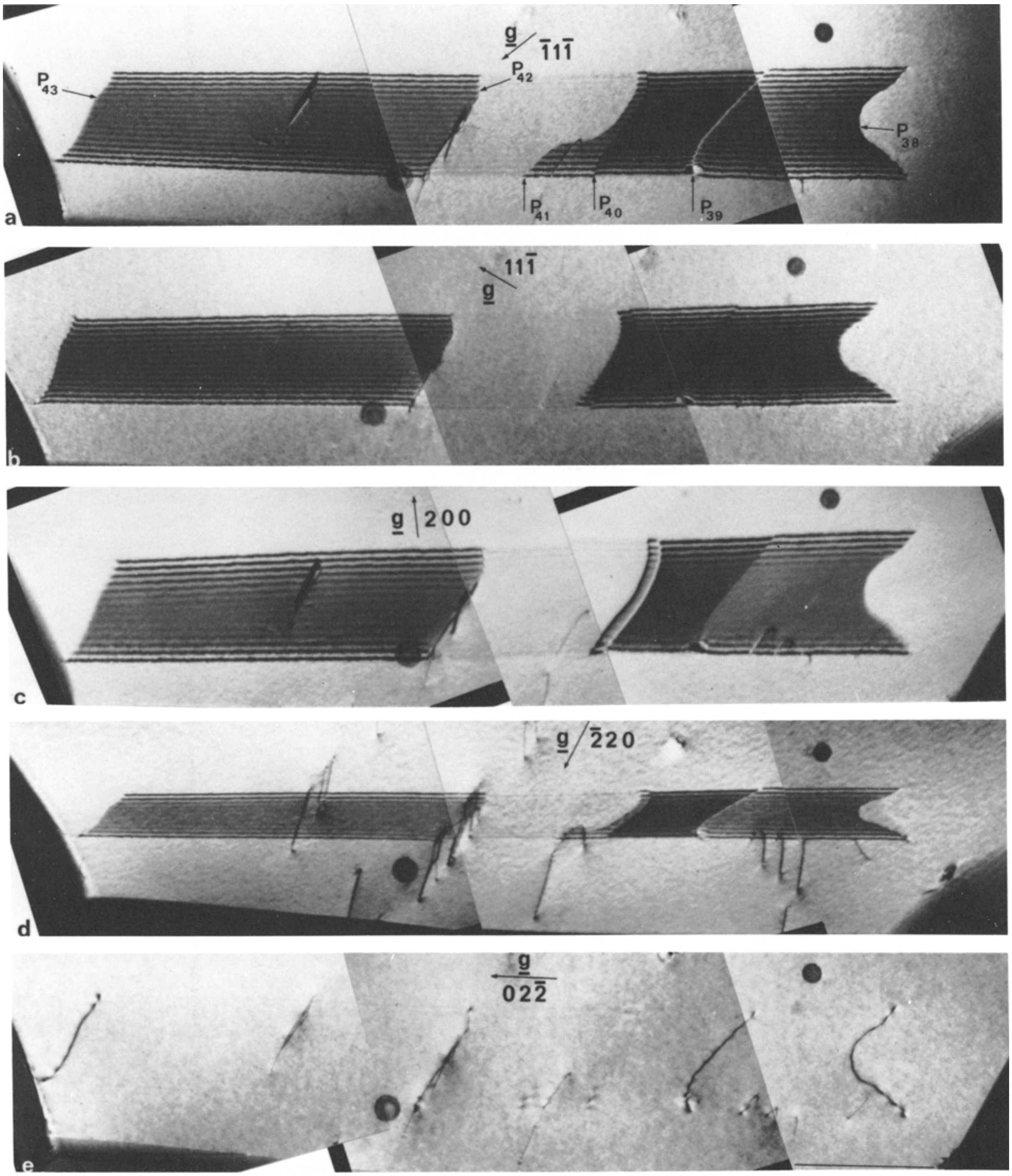

Fig. 7—Micrographs illustrating the contrast behavior of structural features comprising Case IV. The planes of the micrographs (*a*), (*b*), (*c*), (*d*) and (*e*) are ~(011), ~(011), ~(011), ~(111) and ~(011), respectively. The marker represents 1 μ.

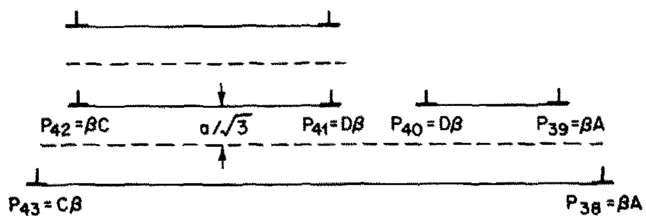

$$A\beta = \frac{a}{6}[\bar{1}1\bar{2}]$$
$$C\beta = \frac{a}{6}[\bar{1}\bar{2}1]$$
$$D\beta = \frac{a}{6}[211]$$

Fig. 8—A possible configurational arrangement of the structural features shown in Fig. 7.

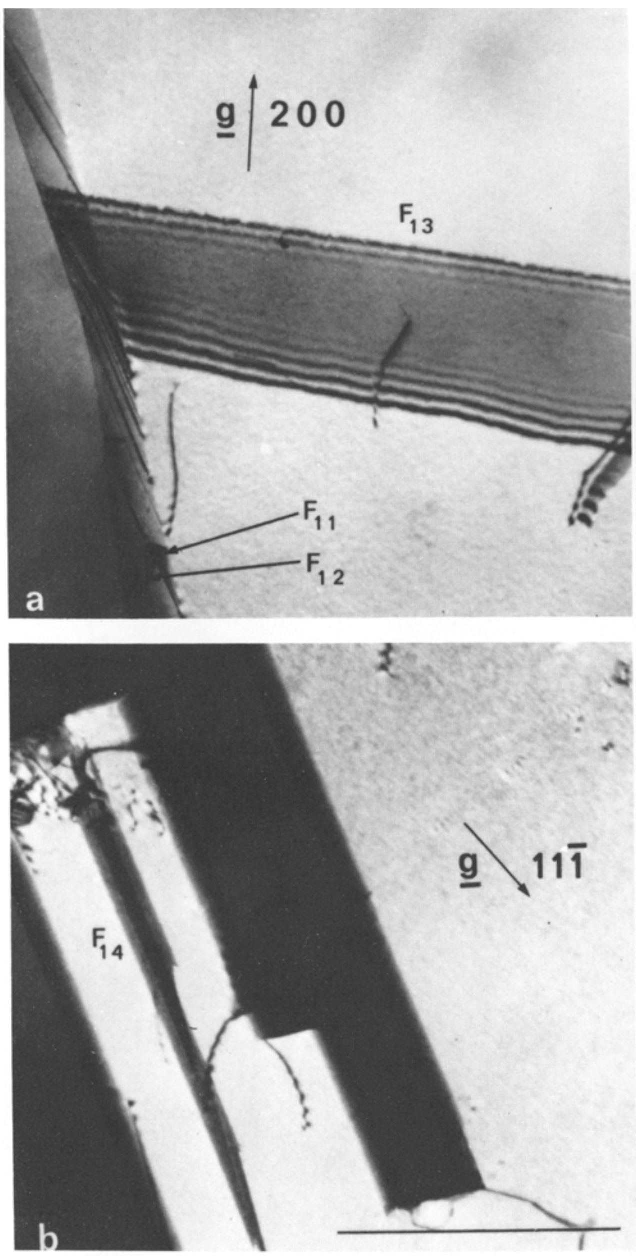

Fig. 9—Micrographs illustrating the role of grain boundaries in the transformations: (*a*) faults nucleating from dislocations residing in the boundary; (*b*) a faulted region nucleating from a noncoherent twin boundary. The plane of the micrograph in each case is ~(011). The marker represents 1 μ.

coherent twin boundary (NCTB) of an annealing twin whose habit is also $(1\bar{1}1)$. It is relatively easy to visualize that, in the case of a noncrystallographic NCTB, the propagation of one out of every two Shockley partials which reside in the interface could produce an HCP crystal.

4.3. Zig-Zag Faults

Fig. 10 shows a relatively rare situation where faults zig-zag between two variants. Coupling the diffraction contrast results presented in Fig. 10 with the single surface trace analysis, the habit planes of F_{15} and F_{16} and F_{17}, F_{18} and F_{19} are identified to be $(1\bar{1}1)$ and $(11\bar{1})$, respectively. Except for F_{17}, interfacial dislocations are not visible in F_{15}, F_{16}, F_{18} and F_{19}, implying that they have no thickness variation.

The possible Burgers vectors of partials bounding F_{17} are $\pm a/6\ [112]$, $\pm a/6\ [\bar{1}21]$ and $\pm a/6\ [2\bar{1}1]$. Since they are in contrast for $\mathbf{g} = \bar{2}20$, the first possibility can be ruled out. However, on the basis of the present experiments, the latter two alternatives cannot be differentiated from each other. For the discussion purposes, we will assume that their Burgers vector is $\pm a/6\ [1\bar{2}\bar{1}]$.

4.4. Evidence for Transformation

Fig. 11(*a*) shows an electron diffraction pattern obtained from an area encompassing F_{15} and the matrix. An extra spot is observed on the pattern, and this cannot be indexed in terms of the $(1\bar{1}1)$ twinning. It can, however, be indexed by assuming that F_{15} is a thin HCP crystal. Since the matrix is oriented along its [011] direction and F_{15} lies on the $(1\bar{1}1)$ plane, it can be shown using transformation matrices[32] that F_{15} should be oriented along its [100] direction, the indices being referred to the three-axes Miller notation for the HCP lattice. Based on this assessment, the observed pattern can be indexed as shown in Fig. 11(*b*).

The diffraction spots from an HCP lattice fall into three categories: i) $h + 2k = 3N + 1$, l odd (where N is an integer); ii) $h + 2k = 3N + 1$, l even; and iii) $h + 2k = 3N$, l even. The presence of the second set of spots implies that a true HCP phase exists.[33] As the 012 spot belongs to this set, it is inferred that F_{15} is a thin HCP crystal lying on the $(1\bar{1}1)$ plane. The observed streaking of the 012 spot in the $[1\bar{1}1]$ direction is consistent with the preceding assessment. Two other extra spots, which are rather weak, are observed in the vicinity of the 012 and $0\bar{2}2$ spots. These could be due to double diffraction.

5. DISCUSSION

It has been demonstrated that, on cooling from 1100°C to room temperature, the alloy undergoes FCC → HCP transformation. Generally, the transformation induced deformation is quite localized, see Figs. 4, 5 and 7. The accompanying microstructures are characterized by the presence of "pseudo" fault pairs, such as F_3, F_4. . . and so forth, and the faulted regions exhibiting light fringes. Two obvious questions arise: i) how these regions evolve; and ii) what role they may have in the transformation. As an illustrative example, consider Case III. It is very likely that an underlying, six-layers HCP region forms first according to the proposed model. When the region grows, the bounding partials are pushed against the CTB between Grains E and F. The presence of dislocation(s) along HI is consistent with this assessment. Subsequently, two glide dislocations with $\pm\mathbf{a}/2$ $[1\bar{1}0]$ and $\pm\mathbf{a}/2$ $[\bar{1}01]$ Burgers vectors interact on the adjacent parallel planes to form a "pseudo" fault-pair delineated by P_{18}, P_{23} and P_{24}. Later on, another $\pm\mathbf{a}/2$ $[\bar{1}01]$ dislocation dissociates in the vicinity of the pseudo fault pair to form an intrinsic fault defined by P_{21} and P_{22}. Since P_{18} and P_{21} have identical Burgers vector, P_{21} may push P_{18} away from P_{23} and P_{24}, resulting in an arrangement shown in Fig. 6. Likewise, other total dislocations within the slipped region may dissociate to form the remaining faults.

A role, identical to the one envisaged in the model, can be assigned to these faulted structures. For example, F_4, F_5, F_6, F_7 and so forth, could be the four-layer HCP nuclei visualized in Fig. 1(b). Furthermore, the observed details regarding the formation of F_6 and F_7 and fault-coalescence are once again consistent with the model.

The manner in which F_{16} blends into F_{17} and F_{19} indicates that they did not form independently. A possible chronological order for their formation could be the following. Assume that the partials bounding F_{15} are gliding from top to bottom in Fig. 10 and their Burgers vector is $\pm\mathbf{a}/6$ $[1\bar{1}\bar{2}]$. The partials bounding a portion of F_{15} could undergo the stair-rod cross slip according to either of the following reactions:

$$\frac{\mathbf{a}}{6}[1\bar{1}\bar{2}]_{(\bar{1}1\bar{1})} \rightarrow \frac{\mathbf{a}}{6}[1\bar{2}\bar{1}]_{(\bar{1}\bar{1}1)} + \frac{\mathbf{a}}{6}[01\bar{1}]_{\text{stair-rod}}$$

$$\frac{\mathbf{a}}{6}[1\bar{1}\bar{2}]_{(\bar{1}1\bar{1})} \rightarrow \frac{\mathbf{a}}{6}[\bar{1}\bar{1}\bar{2}]_{(\bar{1}\bar{1}1)} + \frac{\mathbf{a}}{3}[100]_{\text{stair-rod}}.$$

The propagation of either of the resulting partials, away from the reaction junction, could result in F_{17}. It should however be recognized that the resulting partials constitute an $\mathbf{a}/2$ $[0\bar{1}\bar{1}]$ dislocation in which the $\mathbf{a}/6$ $[1\bar{2}\bar{1}]$ partial leads the $\mathbf{a}/6$ $[\bar{1}\bar{1}\bar{2}]$ partial. Let us assume that F_{17} forms as a result of the $\mathbf{a}/6$ $[1\bar{2}\bar{1}]$

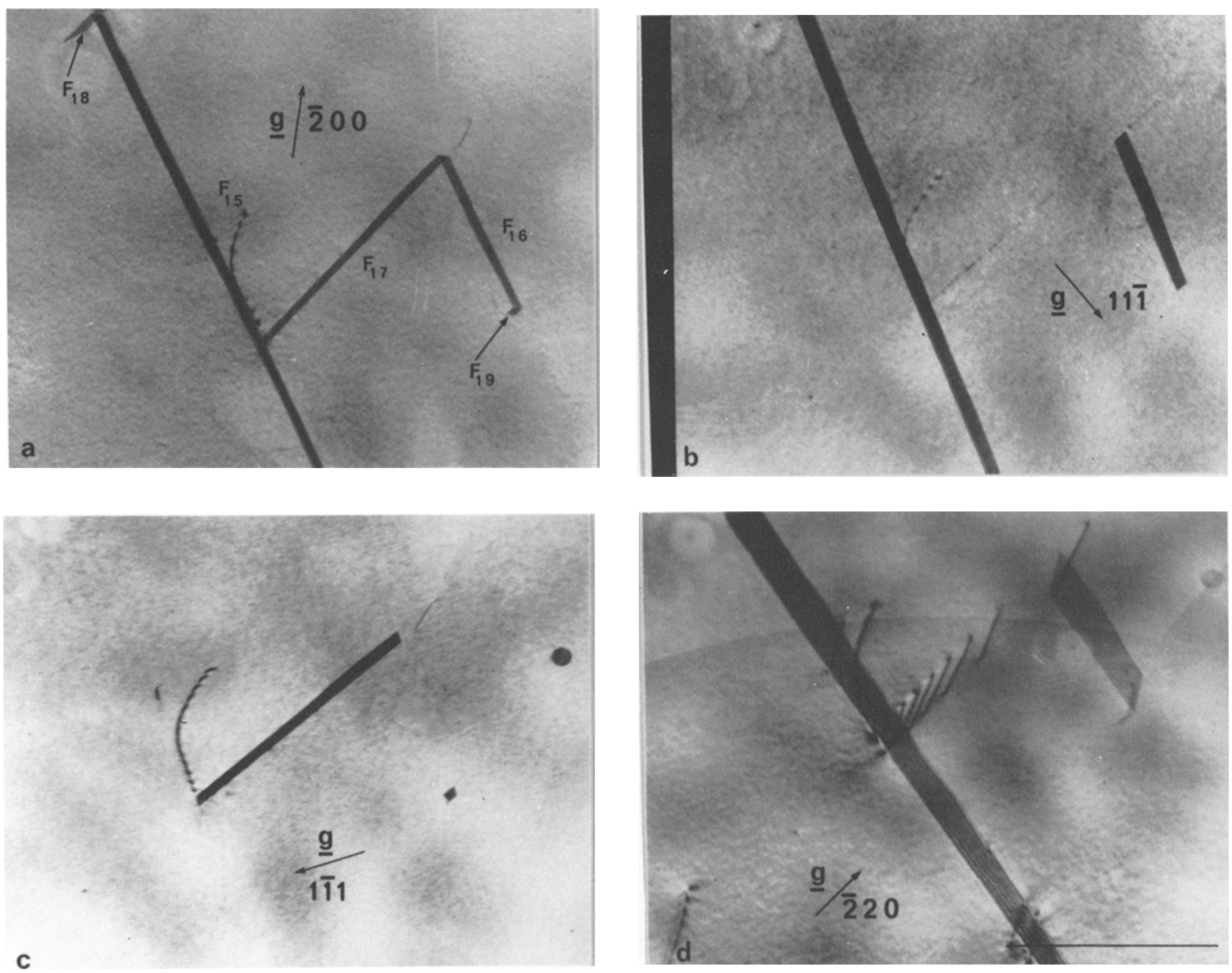

Fig. 10—Micrographs illustrating the contrast behavior of zig-zag faults. The planes of the micrographs (a), (b), (c) and (d) are ~(011), ~(011), ~(011) and ~(111), respectively. The marker represents 1 μ.

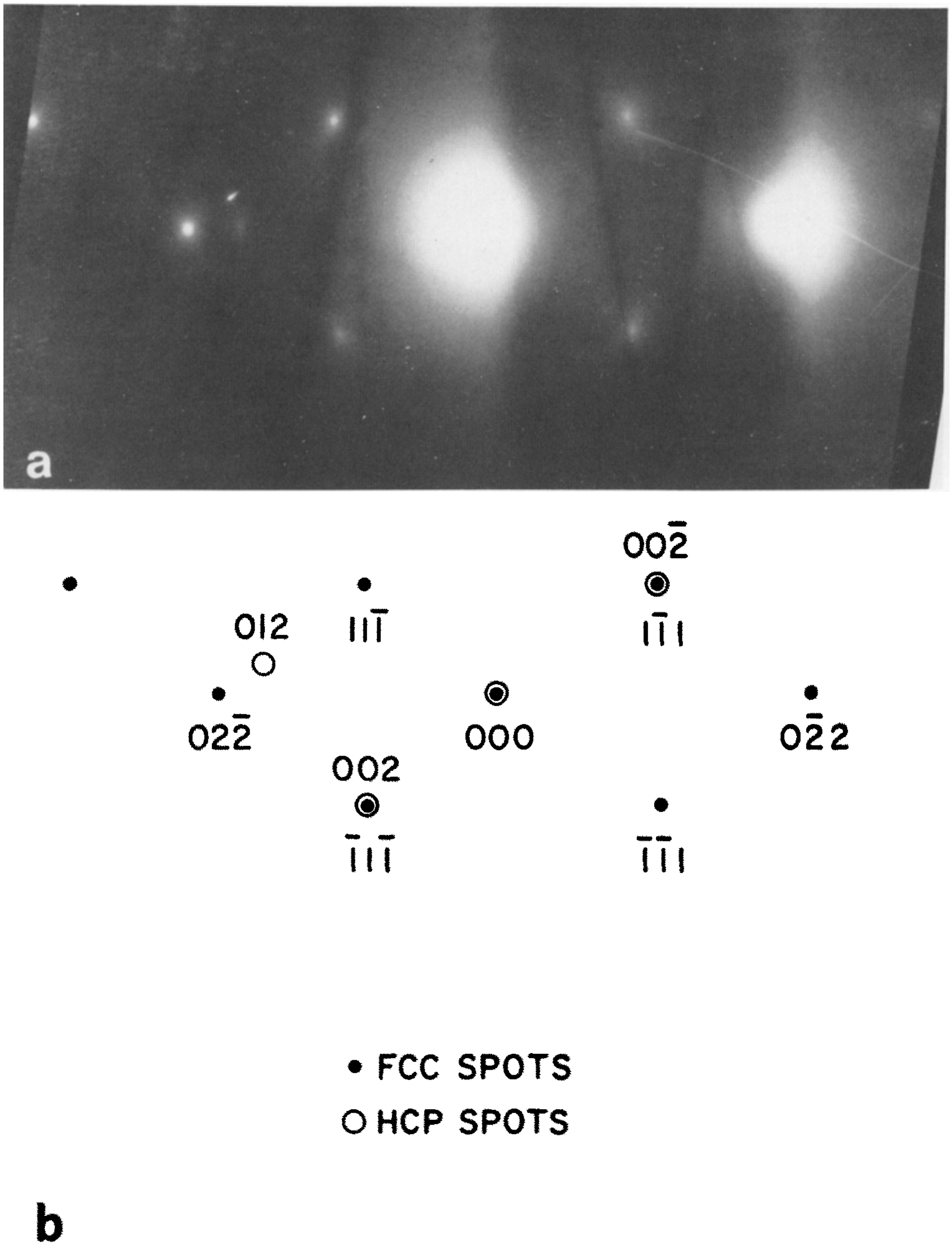

Fig. 11—(*a*) An electron diffraction pattern observed from an area encompassing F_{15} and the matrix. (*b*) The indexed pattern.

slip. Likewise, the $\mathbf{a}/6\ [1\bar{2}\bar{1}]$ partials can dissociate, as follows, to form F_{16}:

$$\frac{\mathbf{a}}{6}[1\bar{2}\bar{1}]_{(\bar{1}\bar{1}1)} \rightarrow \frac{\mathbf{a}}{6}[\bar{1}\bar{2}\bar{1}]_{(\bar{1}1\bar{1})} + \frac{\mathbf{a}}{3}[100]_{\text{stair-rod}}$$

$$\frac{\mathbf{a}}{6}[1\bar{2}\bar{1}]_{(\bar{1}\bar{1}1)} \rightarrow \frac{\mathbf{a}}{6}[1\bar{1}\bar{2}]_{(\bar{1}1\bar{1})} + \frac{\mathbf{a}}{6}[0\bar{1}1]_{\text{stair-rod}}\,.$$

The $\mathbf{a}/6\ [1\bar{1}\bar{2}]$ partials cannot be responsible for F_{16} because their glide from bottom to top would cause anomalous *A*-*A* type stacking. Similarly, it can be argued that F_{19} is caused by the glide of $\mathbf{a}/6\ [\bar{1}\bar{1}\bar{2}]$ partials. If it were not so, F_{17}, F_{16} and F_{19} would enclose a configuration resembling *Z* instead of the observed *C*. Further, the significance of the preceding example, which could be regarded as a modification of the situation envisaged by Fujita and Ueda,[2] in the auto catalytic phenomenon is obvious.

From the present experiments, the role of grain boundaries in the transformation cannot be assessed unequivocally. There are observations which indicate that dislocations residing in the boundary could dissociate into faults, see Fig. 9(*a*). Further, it has previously been observed that CTB's of annealing twins may inherit a network of partial dislocations.[34] If appropriately spaced, these partials could undergo the stair-rod cross slip to form HCP regions. In addition, the propagation of one out of every two partials bounding NCTB's could result in HCP regions.

6. CONCLUSIONS

i) It is envisaged that the nucleation of six-layer HCP regions is governed by the following reaction:

$$\frac{\mathbf{a}}{2}\langle 1\bar{1}0\rangle_{\{111\}} + \frac{\mathbf{a}}{2}\langle 10\bar{1}\rangle_{\{111\}} \rightarrow 3 \times \frac{\mathbf{a}}{6}\langle 2\bar{1}\bar{1}\rangle_{\{111\}}\,.$$

A macroscopic HCP crystal evolves when these nuclei located at different levels within a localized slipped region grow into each other. ii) The observed orientation dependence of the strain-induced martensite as well as the coexistence of HCP and twinned regions can be rationalized in terms of the proposed model. iii) Several substructural features which develop during the early stages of the transformation have been examined in detail by transmission electron microscopy. The circumstantial evidence thus obtained is consistent with the model.

ACKNOWLEDGMENTS

The authors would like to thank G. Y. Chin for introducing them to this unique family of alloys, and also for his constructive comments on the manuscript.

REFERENCES

1. J. W. Christian: *Proc. Roy. Soc.*, 1951, vol. A206, pp. 51-64.
2. H. Fujita and S. Ueda: *Acta Met.*, 1972, vol. 20, pp. 759-67.
3. Z. S. Basinski and J. W. Christian: *Phil. Mag.*, 1953, vol. 44, pp. 791-92.
4. B. A. Bilby: *Phil. Mag.*, 1953, vol. 44, pp. 782-85.
5. A. Seeger: *Z. Metallk.*, 1953, vol. 44, pp. 247-53.
6. A. Seeger: *Z. Metallk.*, 1953, vol. 47, pp. 653-60.
7. W. Bollmann: *Acta Met.*, 1961, vol. 9, pp. 972-75.
8. J. P. Hirth: *Fundamental Aspects of Dislocation Theory*, J. A. Simmons, R. deWit, and R. Bullough, eds., pp. 547-50, National Bureau of Standards, Washington, D.C., 1970.
9. E. deLamotte and C. Altstetter: *Trans. TMS-AIME*, 1969, vol. 245, pp. 651-59.
10. P. S. Kotval and R. W. K. Honeycombe: *Acta Met.*, 1968, vol. 16, pp. 597-607.
11. J. Dash and H. M. Otte: *Acta Met.*, 1963, vol. 11, pp. 1169-78.
12. J. F. Breedis and L. Kaufman: *Met Trans.*, 1971, vol. 2, pp. 2359-71.
13. L. Rémy and A. Pineau: *Met. Trans.*, 1974, vol. 5, pp. 963-65.
14. R. Lagneborg: *Acta Met.*, 1964, vol. 12, pp. 823-43.
15. D. Goodchild, W. T. Roberts, and D. V. Wilson: *Acta Met.*, 1970, vol. 18, pp. 1137-45.
16. G. Stone and G. Thomas: *Met. Trans.*, 1974, vol. 5, pp. 2095-102.
17. S. Mahajan and G. Y. Chin: *Acta Met.*, 1973, vol. 21, pp. 1353-63.
18. S. Mahajan: *Met. Trans. A*, 1975, vol. 6A, pp. 1877-86.
19. C. Nourtier and G. Saada: *Fundamental Aspects of Dislocation Theory*, J. A. Simmons, R. deWit, and R. Bullough, eds., pp. 1259-77, National Bureau of Standards, Washington, D.C., 1970.
20. O. S. Edwards and H. Lipson: *Proc. Roy. Soc.*, 1942, vol. A180, pp. 268-77.
21. A. J. C. Wilson: *Proc. Roy. Soc.*, 1942, vol. A180, pp. 277-85.
22. C. S. Pande and P. M. Hazzledine: *Phil. Mag.*, 1971, vol. 24, pp. 1039-57.
23. J. Friedel: *Dislocations*, pp. 189-90, Addison-Wesley Reading, 1964.
24. J. M. Silcock and W. J. Tunstall: *Phil. Mag.*, 1964, vol. 10, pp. 361-89.
25. W. J. Tunstall and P. J. Goodhew: *Phil. Mag.*, 1966, vol. 13, pp. 1259-72.
26. S. Mahajan: *J. Appl. Phys.*, 1972, vol. 43, pp. 5201-02.
27. A. K. Eikum and D. M. Maher: *Phys. Status Solidi (a)*, 1975, vol. 29, pp. 281-92.
28. H. Hashimoto, A. Howie, and M. J. Whelan: *Proc. Roy. Soc.*, 1962, vol. A269, pp. 80-103.
29. P. Humble: *Phys. Status Solidi*, 1968, vol. 30, pp. 183-92.
30. S. Mahajan: *Phil. Mag.*, 1972, vol. 26. pp. 161-71.
31. S. Mahajan: *Acta Met.*, 1975, vol. 23, pp. 671-84.
32. S. Mahajan, D. Brasen, and T. Wakiyama: Unpublished research, Bell Laboratories, Murray Hill, N.J., 1975.
33. P. B. Hirsch, A. Kelly, and J. W. Menter: *Proc. Phys. Soc.*, 1955 vol. B68, pp. 1132-45.
34. D. E. Barry and S. Mahajan: *Phil. Mag.*, 1971, vol. 23 pp. 727-29.